

1 **Submicron aerosols at thirteen diversified sites in China:**
2 **size distribution, new particle formation and corresponding**
3 **contribution to cloud condensation nuclei production**

4 J.F. Peng¹, M. Hu^{1,*}, Z.B. Wang^{1,‡}, X.F. Huang², P. Kumar^{3, 4}, Z.J. Wu¹, S.
5 Guo¹, D.L. Yue¹, D.J. Shang¹, Z. Zheng¹, L.Y. He²

6 ¹State Key Joint Laboratory of Environmental Simulation and Pollution Control, College of
7 Environmental Sciences and Engineering, Peking University, Beijing 100871, China

8 ²Key Laboratory for Urban Habitat Environmental Science and Technology, School of
9 Environment and Energy, Peking University Shenzhen Graduate School, Shenzhen 518055,
10 China

11 ³Department of Civil and Environmental Engineering, Faculty of Engineering and Physical
12 Sciences (FEPS), University of Surrey, Guildford GU2 7XH, United Kingdom

13 ⁴Environmental Flow (EnFlo) Research Centre, FEPS, University of Surrey, Guildford GU2
14 7XH, United Kingdom

15 [‡]Now at: Multiphase Chemistry Department, Max Planck Institute for Chemistry, Mainz 55128,
16 Germany

17 *Correspondence to: M. Hu (minhu@pku.edu.cn)

18 **Abstract**

19 Understanding the particle number size distributions in diversified atmospheric
20 environments is important in order to design mitigation strategies related to submicron
21 particles and their effects on regional air quality, haze and human health. In this study,
22 we conducted 15 different field measurement campaigns between 2007 and 2011 at 13
23 individual sites in China, including 5 urban sites, 4 regional sites, 3 coastal/background
24 sites and one ship cruise measurement along eastern coastline of China. Size resolved

25 particles were measured in the 15-600 nm size range. The median particle number
26 concentrations (PNCs) were found to vary in the range of $1.1\text{-}2.2 \times 10^4 \text{ cm}^{-3}$ at urban
27 sites, $0.8\text{-}1.5 \times 10^4 \text{ cm}^{-3}$ at regional sites, $0.4\text{-}0.6 \times 10^4 \text{ cm}^{-3}$ at coastal/background sites,
28 and $0.5 \times 10^4 \text{ cm}^{-3}$ during cruise measurement. Peak diameters at each of these sites
29 varied greatly from 24 nm to 115 nm. Particles in the 15-25 nm (nucleation mode), 25-
30 100 nm (Aitken mode) and 100-600 nm (accumulation mode) range showed different
31 characteristics at each sites, indicating the features of primary emissions and secondary
32 formation in these diversified atmospheric environments. Diurnal variations show a
33 build-up of accumulation mode particles belt at regional sites, suggesting the
34 contribution of regional secondary aerosol pollution. Frequencies of new particle
35 formation (NPF) events were much higher at urban and regional sites than at coastal
36 sites and cruise measurement. The average growth rates (GRs) of nucleation mode
37 particles were $8.0\text{-}10.9 \text{ nm h}^{-1}$ at urban sites, $7.4\text{-}13.6 \text{ nm h}^{-1}$ at regional sites and 2.8-
38 7.5 nm h^{-1} at coastal sites and cruise measurement. The high gaseous precursors and
39 strong oxidation at urban and regional sites not only favored the formation of particles,
40 but also accelerated the growth rate of the nucleation mode particles. No significant
41 difference in condensation sink (CS) during NPF days were observed among different
42 site types, suggesting that the NPF events in background areas were more influenced
43 by the pollutant transport. In addition, average contributions of NPF events to potential
44 cloud condensation nuclei (CCN) at 0.2% super-saturation in the afternoon of all
45 sampling days were calculated as 11% and 6% at urban sites and regional sites,
46 respectively. On the other hand, NPF events at coastal sites and cruise measurement
47 had little impact on potential production of CCN. This study provides a large dataset of
48 particle size distribution in diversified atmosphere of China, improving our general
49 understanding of emission, secondary formation, new particle formation and
50 corresponding CCN activity of submicron aerosols in Chinese environments.

51 **Key words:** Submicron aerosols; Size distribution; New particle formation; Cloud
52 condensation nuclei

53

54 **1 Introduction**

55 Atmospheric particles play an important role in the degradation of visibility and
56 changing the balance of global radiative forcing (Dusek, 2006; IPCC, 2007), besides
57 showing adverse impacts on human health (Heal et al., 2012). Size of atmospheric
58 particles, ranging from 1.5 nm up to hundreds of micrometers, is a key factor for
59 evaluating environmental effects of particles (*Kulmala et al., 2013; Buseck and Adachi,*
60 *2008; Kumar et al., 2014*). For example, particle diameter is considered to be more
61 important than chemical composition for cloud-nucleating ability (*Dusek, 2006*).
62 Smaller particles may have greater potential of health impacts compared with their
63 larger counterparts (*WHO, 2013*). Particles smaller than 100 nm in diameter (ultrafine
64 particles) have deeper deposition in human body and are able to induce more intense
65 oxidative stress in cells (*Nel et al., 2006*). Accumulation mode particles, on the other
66 hand, have high light extinction efficiency and can explain degradation of visibility in
67 severe air pollution event to a great extent (*See et al., 2006*). Meanwhile, particle size
68 distribution offers information on type, origin, and atmospheric transformation of the
69 particles (*Buseck and Adachi, 2008; Harrison et al., 2011*). Therefore, the knowledge
70 of size distributions of submicron particles, including their temporal and spatial
71 variability, is crucial in characterizing human exposure, estimating climate effects, and
72 designing monitoring strategies for both developed and developing countries (*Kumar*
73 *et al., 2014*).

74 Measurements of particle number distribution (PND) have been extensively
75 conducted in many European and US sites in the past two decades (*Asmi et al., 2011a;*
76 *Bigi and Ghermandi, 2011; Borsos et al., 2012; Kumar et al., 2010; Wehner and*
77 *Wiedensohler, 2003*), but at a much lesser extent in developing countries (*Monkkonen*
78 *et al., 2005; Wu et al., 2008; Kumar et al., 2011; Wang et al., 2013a,b*). Temporal and
79 spatial variation of PND in these developed countries has been widely recognized (*Asmi*
80 *et al., 2011a*). Whilst these particles arise from a number of non-vehicle exhaust sources
81 (*Kumar et al., 2013b*), primary emission from road vehicles is thought to be a main
82 source of particle number concentration (PNC) in urban areas (*Kumar et al., 2010*).

83 The new particle formation (NPF), associated with a rapid burst of nucleation mode
84 particles, results in an increase of CCN number concentration after growth
85 (*Wiedensohler et al.*, 2009). The NPF events were observed in many atmospheric
86 environments in the world, especially in relatively clean atmosphere (*Kulmala et al.*,
87 2013). Though the first study on NPF events during polluted episodes was conducted
88 in the megacity of Beijing (*Wehner et al.*, 2004; *Wu et al.*, 2007), the occurrence of NPF
89 events is only reported at a few sites in China up to now (*Du et al.*, 2012; *Liu et al.*,
90 2008; *Wang et al.*, 2013c; *Wehner et al.*, 2004; *Wiedensohler et al.*, 2009; *Herrmann et*
91 *al.*, 2014). Although it is a common interest that regional NPF events are a main source
92 of atmospheric CCN production (*Kuang et al.*, 2009), most of the estimation on the
93 contribution of NPF events to CCN concentration till date are only based on model
94 simulations using regional/global scale models with extra NPF mode (*Merikanto et al.*,
95 2009; *Yu et al.*, 2012). The only few measurement studies that attempted to quantify the
96 strength of this nucleation process merely calculated the enhancement of CCN
97 concentration along with NPF events (*Yue et al.*, 2011; *Kerminen et al.*, 2012; *Kuang et*
98 *al.*, 2009; *Asmi et al.*, 2011b). These enhancement results are likely to be greatly
99 influenced by factors such as change of boundary layer as well as primary emissions.
100 More measurements and new measurement-based approaches are therefore needed to
101 estimate the contribution of NPF to corresponding CCN concentration in diversified
102 environments.

103 China has been experiencing unprecedented modernization and urbanization
104 process since 1980s. The rapid industrial revolution has intensively occurred in China
105 during the past 30 years, providing both the chance to become “the world factory” and
106 the challenge of severe air pollution problem. The aerosol pollution in recent years at
107 both local and regional scale has attracted great attention, as it results in the heavy smog
108 or haze episodes and might lead to potential health effects (*Xu et al.*, 2013). The aerosol
109 pollution characterizes regional property in major economic developed regions with
110 megacity or city clusters, for instance, Bohai Sea Rim Region, Yangtze River Delta and
111 Pearl River Delta. To understand the feature of aerosol pollution in these regions

112 requires multi-site measurements within each pollution region.

113 In this study, we have therefore conducted PND measurements at 13 different sites
114 in China in order to provide comprehensive understanding of the effects of primary
115 emissions, regional pollutants transportation and new particle formation on PNDs.
116 These sites are classified into four main categories – urban, regional, coastal and ship
117 cruising – representing the typical atmospheric environments in China. Unique features
118 of each site category, including the particle size distributions, seasonal and diurnal
119 variation, are discussed in this paper. Special focus is given to the NPF events and their
120 contribution to CCN concentration at each of the thirteen sites.

121 **2 Methodology**

122 **2.1 Sites description**

123 A total of 15 field measurement campaigns of PNDs were conducted at 13 different
124 sites between 2007 and 2011. These sites were broadly classified in the following four
125 types of atmospheric environment categories (see Table 1), including five urban sites,
126 four regional sites, three coastal/ background sites and one ship cruise measurement
127 along Eastern coastal China . As shown in Fig. 1, most of these sites were situated in
128 the most developed and largest city cluster regions in China.

129 *2.1.1 Urban sites*

130 The first urban site, Guangzhou (GZ_u; 23.13° N, 113.26° E) was located on the roof
131 of the Guangdong Provincial Environmental Monitoring Center in the downtown of
132 Guangzhou city, at a height of about 50 m above street level (Yue *et al.*, 2013). This site
133 is representative of a typical ambient condition in Guangzhou urban areas (Zhang *et al.*,
134 2008).

135 The second urban site, Shanghai (SH_u; 21.53° E, 31.23° N), was located on the roof
136 of a 6-floor building of Shanghai Pudong Environmental Monitoring Station in the
137 eastern part of Shanghai urban areas. The surroundings of this site were mainly
138 residential and business buildings (Huang *et al.*, 2012).

139 The third urban site, Urumchi (UR_u ; $87.58^\circ N$, $43.83^\circ E$), was located on roof of the
140 Urumchi Environmental Monitoring Center in the downtown of Urumchi city. Urumchi
141 city is the capital of Xinjiang Uyghur Autonomous Region, with the biggest desert in
142 China to the north and mountains to the south. Sampling inlet at UR_u site was located
143 at ~ 20 m above the street level. The surroundings were mainly residential and business
144 buildings. There was one main road 200 m away to the west and another 400 m away
145 to the east.

146 The fourth urban site, Wuxi (WX_u ; $31.56^\circ N$, $120.29^\circ E$), was located on the roof
147 of a five-floor building in the center of Wuxi City. This site was surrounded by the
148 residential buildings. No obvious stationary sources existed nearby and the nearest main
149 road was about 300 meters away to the east. The sampling inlet was at ~ 15 m above the
150 ground level.

151 The fifth urban site, Jinhua (JH_u ; $29.1^\circ N$, $119.69^\circ E$), was located on the roof of
152 the Jindong Environmental Building in the east part of the city of Jinhua. The sampling
153 inlet was at ~ 25 m above the street level. There was no industry source nearby and the
154 nearest main road was located ~ 300 m away to the west. As the wind direction is always
155 from northeast during the measurements (October), the influence of this main road on
156 our site can be ignored.

157 2.1.2. Regional sites

158 The first regional site, Heshan (HS_r ; $22.71^\circ N$, $112.93^\circ E$), was an urban outflow
159 site of Guangzhou megacity in central Pearl River Delta (PRD), with a distance from
160 Guangzhou downtown 50 km. It was located on the top of a small hill (40 m), about 7
161 km away from Heshan downtown areas, and was far from strong industrial sources. The
162 surrounding areas of the site were dominated by farmlands and forests. Biomass
163 burning events were observed occasionally in the farmlands. This site can be well
164 representative of the air pollution outflow from the polluted central PRD urban areas
165 (*Gong et al.*, 2012).

166 The second regional site, Kaiping (KP_r ; $22.33^\circ N$, $112.54^\circ E$), was located ~ 120

167 km away from the city of Guangzhou to the southwest. Under the influence of the Asian
168 monsoon, the dominant air mass comes to PRD from the northeast in fall. Hence, the
169 Kaiping site could be assumed to be a downwind receptor site. Instruments were placed
170 on the third floor of the building at the Kaiping supersite (~10 m above the ground
171 level), which is surrounded by shrubs and eucalyptus forest (*Wang et al.*, 2013c). The
172 site was free of any significant local pollution emissions. A detailed geographic
173 description of this measurement site can be seen elsewhere (*Huang et al.*, 2011).

174 The third regional site, Jiaxing (JX_r; 30.8 ° N, 120.8 ° E), was a suburban site
175 between Shanghai and Hangzhou. It was located on the roof of school building in a
176 small town, 15 m above the ground level and 8 km away from the downtown of Jiaxing
177 city, which was situated in the middle of Shanghai megacity and Hangzhou, capital of
178 Zhejiang province.

179 The fourth regional site, Yufa (YF_r; 39.51 ° N, 116.3 ° E), was about 40 km to the
180 south of Beijing downtown area. This site was located on top of a building (~20 m
181 above the ground level) at the campus of Huangpu College. There was no industrial
182 sources around this site, except the farm land and a residential area (*Guo et al.*, 2010).

183 2.1.3 Three coastal/ background sites

184 The first coastal site, Baguang (BG_c; 22.65 ° N, 114.54 ° E), was located on the roof
185 of a three-floor building (~10 m above sea level) at the seaside in a small peninsula in
186 the southern China, 50 km away from the city of Shenzhen to the east. No stationary
187 source or traffic source was found nearby the site. To the east and south of the site was
188 the South China Sea. This site can well represent the background atmosphere of
189 southern China during autumn.

190 The second coastal site, Wenling (WL_c; 28.40 ° N, 121.61 ° E), was situated in a
191 flat ground area in a peninsula in the southeast of China, surrounding by only farmland.
192 The sampling inlet was about 4 m above the ground level. The East China Sea was up
193 to 2 km away from the site to the northeast and southeast. The city of Taizhou was about
194 30 km away to the northwest of the site. Wind direction ranged from north to east during

195 the whole campaign at WL_c site, resulting in a variety of air masses that can be
196 encountered from modified clean maritime air mass to polluted continental air mass.

197 The third coastal site, Changdao (CD_c; 37.99 °N, 120.70 °E), was located at ~50 m
198 above the sea level on a hill in the north coast of an island. This island lied offshore to
199 the east edge of central eastern China and laid between the Jiaodong and the Liaodong
200 Peninsula in the Bohai Sea, called Changdao. The Changdao Island was surrounded by
201 sea on three sides and connected with a larger island by a bridge on the south side. A
202 detailed geographic description of the measurement site is presented in (*Hu et al.*, 2013).

203 2.1.4 Ship cruise measurement

204 Ship cruise measurement (ES_s) was carried out on the “Dong Fang Hong 2”,
205 which is a multi-functional marine research vessel
206 (<http://eweb.ouc.edu.cn/4b/61/c4169a19297/page.htm>). The observatory was located
207 on the 6th floor of the “Dong Fang Hong 2”, which was about 15 m above the sea level.
208 The vessel sailed from Qingdao of Shandong province (24.5 °N, 118.1 °E) on March 17th,
209 reached the southernmost area of the cruise near Wenzhou of Zhejiang province on
210 March 27th, and returned at Qingdao (24.5 °N, 118.1 °E) on April 9th. The study area of
211 the whole cruise covered both the East China Sea and Yellow Sea of China (see Figure
212 1).

213 2.2 Instrumentation

214 The Scanning Mobility Particle Sizer (SMPS, TSI Inc.) system was used to obtain
215 PNDs in the 15-600 nm (mobility diameter) size range at all the 13 sites. The SMPS
216 system includes one Differential Mobility Analyzer (DMA) and one Condensation
217 Particle Counter (CPC). The time resolution of this system was 5 min and the flow rates
218 of sample and sheath air were 0.3 and 3.0 L/min, respectively. The relative humidity of
219 sample air was kept below 40% by a silica diffusion dryer within the inlet lines and
220 sheath air cycles. Size-dependent particle losses inside the instruments as well as in the
221 sampling tubes are calculated (*Willeke*, 1993), and the data are corrected by the obtained
222 correction parameters for each site.

223 **2.3 Parameterization**

224 PNDs at each site are parameterized by a multiple log-normal distribution function.
 225 Each mode is described by the following function (*Seinfeld and Pandis, 1998*):

$$226 \quad \frac{dN_i}{d\log D_p} = \frac{N_i}{\sqrt{2\pi}\log\sigma_i} \exp\left[-\frac{(\log D_p - \log\mu_i)^2}{2(\log\sigma_i)^2}\right] \quad (1)$$

227 Where N_i , μ_i and σ_i are the total number concentration, mean diameter and geometric
 228 mean standard deviation of the distribution of mode i , respectively. The task of the
 229 fitting program is to minimize the residual part Q, which is described as:

$$230 \quad Q = \int_{15}^{600} \frac{|dN/d\log D_p - \sum_i dN_i/d\log D_p|}{dN/d\log D_p} d\log D_p \quad (2)$$

231 The growth rate (GR) of newly formed particles and condensational sink (CS) are
 232 calculated for NPF events. The CS determines the how quickly of the gaseous
 233 molecules can condense onto the pre-existing aerosols and can be calculated by using
 234 Equation (3) (*Kulmala et al., 2001, 2012*).

$$235 \quad CS = 2\pi D \int_{15}^{600} D_p \beta_M(D_p) n(D_p) d\log D_p = 2\pi D \sum_i \beta_M D_{p,i} N_i \quad (3)$$

236 Here D is the diffusion coefficient; $n(D_p)$ represents the dry particle size distribution
 237 function; β_M is the transitional correction factor for the mass flux; and N_i is the particle
 238 number concentration in the size section i . The CS value in NPF days is calculated as
 239 the mean value between 9:00 to 12:00 h (local time) of the day. It should be noted that
 240 the CS values calculated here are based on the dry particle number size distributions,
 241 which may underestimate the real CS values in ambient humidity.

242 GR is calculated using the Equation (4) (*Kulmala et al., 2012*):

$$243 \quad GR = \frac{\Delta D_{p,m}}{\Delta t} \quad (4)$$

244 Where $D_{p,m}$ is a mean geometric diameter resulted from the log-normal fitting of the
245 particle number size distribution. The methods for calculating both CS and GR are
246 described by Wu et al. (2007).

247 The critical diameter ($D_{p,crit}$) at which 50% of the particles are activated at the super
248 saturation (S_c) can be calculated based on the knowledge of ambient Kappa (κ) value
249 expressed by Eq. (5) (Petters and Kreidenweis, 2007).

$$250 \quad \kappa = \frac{4A^3}{27D_{p,crit}^3 \ln^2 S_c} \quad (5)$$

$$251 \quad A = \frac{4\sigma_{s/a} M_w}{RT\rho_w} \quad (6)$$

252 Where κ is the hygroscopicity parameter used to model the composition-dependence of
253 the solution water activity; $\sigma_{s/a}$ is the droplet surface tension (assumed to be that of pure
254 water with a value of 0.0728 N m⁻²); M_w is the molecular weight of water; ρ_w is the
255 density of liquid water (g cm⁻³); R is the universal gas constant (J mol⁻¹K⁻¹), and T is the
256 absolute temperature (K).

257 **3 Results and discussion**

258 **3.1 Spatial and seasonal variability of PND**

259 The statistics of PNC in the 15-600 nm size range are given in Table 2. Average
260 and median PNCs at all sites were in the range of 0.5-2.8 ×10⁴ cm⁻³ and 0.4-2.2 ×10⁴
261 cm⁻³, respectively. The median PNC at urban (1.1-2.2 ×10⁴ cm⁻³) and regional sites (0.8-
262 1.5 ×10⁴ cm⁻³) were two-times larger than those at coastal/background (0.4-0.6 ×10⁴
263 cm⁻³) and cruise measurement (0.5 ×10⁴ cm⁻³). The highest PNCs were observed at UR_u
264 site due to frequent NPF events, as well as intensive primary emissions, such as coal
265 combustions for local industries, heating supply and residents' use (Li et al., 2008). The
266 average observed PNCs at Chinese urban sites (1.8×10⁴ cm⁻³) were higher than those in
267 European cities which were reported as 1.6-7.0 ×10³ cm⁻³ and 1.6±0.8 ×10⁴ cm⁻³ by
268 Borsos et al. (2012) and Kumar et al. (2013a), respectively, suggesting a much larger

269 exposure risks to Chinese population compared with those in European cities.
270 Meanwhile, the average PNCs in low aerosol-loading area (coastal/background sites)
271 in China were still two-fold higher than those in European countries (*Asmi et al.*, 2011a).
272 This suggests that the high aerosol loading in the background areas of China increases
273 the background aerosol concentration.

274 Peak diameters for measured size distributions are calculated in the range of 24-
275 123 nm at all sites (Table 2). The peak diameters were found higher at regional sites
276 (89 nm on average) than at urban sites (69 nm on average). Aging of particles during
277 their transport from urban to regional area likely leads to the growth of particle
278 diameters (*Moffet and Prather*, 2009), which leads to the largest particle peak diameters
279 at regional sites despite the frequent NPF events at these sites. Besides, particle
280 emissions from biomass burning in regional areas have diameter larger than 100 nm
281 (*Reid et al.*, 2005), and may influence the diameter of ambient particles at regional sites.
282 At coastal sites, the peaks of particle size distributions were not as sharp as those seen
283 at other sites (Fig. 2). The PNCs show a wide variation near the peak diameters, as both
284 clean background episodes and polluted episodes caused by transportation occurred in
285 these areas (*Hu et al.*, 2013).

286 The median particle size distribution at most of the sites can be fitted into three
287 modes. The peak diameters of these modes were in the range of 132-327 nm for the
288 first mode (which can be roughly recognized as accumulation mode), 59-116 nm for
289 the second mode (which can be roughly recognized as Aitken mode), and 17-38 nm for
290 the third mode (which can be roughly recognized as nucleation mode or the second
291 Aitken mode) (Table 2). At HS_r, CD_r and ES_s sites, the fitting exercises give only the
292 first and second modes.

293 Strong seasonal variations were found at JX_u and WX_u sites, where measurements
294 were conducted both in summer and winter. Higher PNCs in nucleation mode and lower
295 PNCs in accumulation mode were observed in summer measurements.

296 **3.2 Particle number concentration in different size ranges**

297 The PNCs in the 15-600 nm range are separated into three different size groups,
298 which are smaller than 25 nm (N_{15-25}), 25-100 nm (N_{25-100}) and 100-600 nm ($N_{100-600}$).
299 These three size groups are used to represent three modes of nucleation, Aitken, and
300 accumulation, respectively. The number concentration in each mode can be
301 approximated by integrating certain size distribution using the Equation (7):

$$302 \quad N_{a-b}(t) = \int_a^b n(D_p, t) d\log D_p = \sum_{i=a}^b n_i(D_p, t) \quad (7)$$

303 Where $N_{a-b}(t)$ represents PNCs in the a-b nm range at a certain time interval, D_p is
304 the geometric mean diameter of the size interval, and n_i is the measured PNC in a
305 particular size interval (cm^{-3}).

306 As illustrated in Figure 3, the PNCs in each size range show a good log-normal
307 distribution in most cases, but there are still several major differences among the
308 distribution of PNCs in different size ranges at individual sites. The $N_{100-600}$ at urban
309 and regional sites were much larger than those at coastal sites and cruise measurement,
310 though these values did not show obvious differences between urban and regional sites,
311 indicating the regional feature of secondary aerosols in the whole region of city clusters.
312 Mean N_{25-100} values appeared to be up to 10-times higher than those in 100-600 nm size
313 range at urban sites, but no significant difference was found at other sites (figure 3),
314 suggesting the emission from road vehicles at urban sites. The distributions of both N_{15-}
315 25 and N_{25-100} show a very “narrow” distribution at most studying sites compared with
316 European countries (*Asmi et al.*, 2011a), mainly because there was seldom clean
317 episodes with very few particles in the atmosphere in China. Even if the air mass was
318 coming from the clean remote continental or oceanic region, the new particle formation
319 and high flux of primary particle emission would increase the N_{15-25} and N_{25-100} within
320 a short time (*Wu et al.*, 2008). The PNCs of nucleation mode (N_{15-25}) particles at coastal
321 sites were lower than those of $N_{100-600}$ and N_{25-100} , especially in autumn and winter,
322 suggesting that either the nucleation rate was low, or high proportion of nucleation
323 mode particles coagulated onto the surfaces of larger particles. Besides, a “wide”

324 distribution (figure 3c) of N_{15-25} indicates that though the nucleation rate was low most
325 of time at coastal sites, a few NPF events with high concentration in nucleation mode
326 still occurred.

327 **3.3 Diurnal variation of PND**

328 Fig. 4 shows the diurnal variations of the average PND at all the measurement sites.
329 These figures are sorted by seasons and site types. Diurnal PND at nearly all the
330 measurement sites presents a build-up of high concentration belts with peak diameter
331 between 70 and 150 nm. These belts were much more obvious during night time, when
332 there was neither NPF event nor large amount of primary emissions, and should be
333 recognized as the accumulation mode. As smaller particles in nucleation mode and
334 Aitken mode have large diffusion coefficient which provide them a large possibility to
335 coagulate onto the surfaces of larger-sized particles, the residence time for particles in
336 the boundary layer are short (*Davidson and Wu, 1990*). On the other hand, accumulation
337 mode particles had much longer atmospheric life and experienced longer aging process
338 in the atmosphere, resulting in the appearance of this accumulation belt. The higher
339 concentration and larger diameter of particles in this accumulation belts may reflect
340 higher degree of aging of ambient particles. For example, at some sites such as YF_r and
341 KP_r , the peaks of these layers were about 100-120 nm, larger than those at the urban
342 sites of SH_u and WX_u (about 80-90 nm). Besides, particles at all other sites in the three
343 large city groups (see the black circle in Figure 1) had these high concentration belts,
344 suggesting that the regional pollution feature within the whole city group area. In
345 contrast, no such accumulation belt was found at UR_u site, as the PND at UR_u site was
346 largely influenced by the large primary emissions and NPF.

347 There were large concentrations of nucleation mode particles in the middle of the
348 day at most of studying sites (Figure 4), showing the contribution of the NPF events to
349 the PNC during the whole measurements. The contributions to the PNCs were much
350 more obvious in summer time due to much more NPF events. On the other hand, the
351 PNCs of nucleation mode were pretty low at any time of day during both the winter

352 measurement campaigns and some of the autumn measurements since there was no
353 NPF event found (Table 3). Compared with urban and regional sites, influence of PNC
354 at coastal/background sites by NPF events was much lower due to the lower
355 concentration of precursor gases (e.g. SO₂) at these sites.

356 Besides the peak of NPF events around the noon, there were another two
357 concentration peaks during morning (between 07:00 and 09:00 h) and evening (between
358 17:00 and 20:00 h) rush hours at most of the urban sites, with the size of the peaks about
359 30-70 nm. The appearance of these peaks was due to the primary emissions from
360 vehicles as well as the diurnal change of the height of boundary layers (*Lin et al.*, 2009).
361 In the meanwhile, at regional sites there were also two concentration peaks at the same
362 time of day. The difference is that at regional sites the sizes of these peaks were much
363 larger (about 70-150 nm) than at urban sites. This reveals the fact that biomass burning
364 in the regional farmland contribute large amount of primary particles (*Huang et al.*,
365 2011; *Reid et al.*, 2005). Besides, such morning and evening peaks were not found at
366 coastal sites, confirming that there was no primary emission near these coastal sites.

367 **3.4 Frequencies and parameters of NPF events**

368 Obvious NPF events were recognized during most of our measurements. The
369 criterion for discerning NPF events in this study includes three steps. First, there should
370 be a burst of PNC in nucleation mode (below 25 nm in diameter) (*Birmili and*
371 *Wiedensohler*, 2000). Second, primary emitted species, such as black carbon and CO
372 concentrations should not enhance significantly. Third, the event should last for more
373 than 2 hours, with the increase in particle diameter. As the lower cut-off diameter of our
374 measurements was 15 nm, which is much larger than the size of nucleation clusters
375 (1.5-2 nm) (*Kulmala et al.*, 2013), the NPF events might occur 1 to 2 hours before we
376 observed them. Two typical types of NPF events (the “banana” and the “apple”, which
377 were classified by *Wu et al* (2007)) were observed at a number of our sites. The
378 frequencies of NPF events at urban and regional sites (38%) were similar to previous
379 studies that focused on the NPF events in some other sites in China (*Wu et al.*, 2007;
380 *Yue et al.*, 2013) and were much higher than at coastal sites and cruise measurement

381 (14%) during our measurements (Figure 5).

382 Sulfuric acid is a well-known precursor for nucleation (*Boy et al., 2005; Zhang,*
383 *2010; Yue et al., 2010; Andreae, 2013*). High concentrations of SO₂ and OH provide
384 strong source of sulfuric acid at urban and regional sites, and promote the NPF events.
385 On the other hand, the aerosol loading in the ambient atmosphere acts as the
386 condensation and coagulation sink and thus restrains the NPF event. Though the high
387 concentration of pre-existing particles can hinder the NPF in urban and regional areas,
388 there will also be high precursor concentration (such as SO₂, and VOCs) and strong
389 oxidation (performed as high O₃ and OH radical concentration) in these areas, which
390 will favor the NPF. At urban and regional sites in our study, the high precursor
391 concentration and strong oxidation may play a more crucial role than the high
392 concentration of pre-existing particles, leading to the high frequency of NPF events. On
393 the other hand, in the clean coastal area in China, concentrations of precursors as well
394 as the particles are not as high as in urban area as both gases and particles will be dilute
395 during the transport from polluted region to clean coastal area. However, unlike the
396 particles, the gaseous precursors may also undergo continually atmospheric oxidation
397 and transform into particle phase during the transport, which makes the reduction of
398 gaseous precursors larger than the reduction of particles, resulting in fewer NPF events
399 at coastal sites. Besides, other reasons such as meteorological conditions might also
400 affect the frequency of NPF events at diversified sites. In polluted areas, the NPF events
401 are often expected to occur since the air mass is coming from the clean continental
402 background and is not greatly influenced by the polluted urban air (*Wu et al., 2007*). At
403 coastal sites, however, no NPF events were noted when the air mass was coming from
404 the ocean side with clean air, as this cleaner air mass was not carrying enough NPF
405 precursors such as H₂SO₄ or low-volatile VOCs to favor the nucleation events. This is
406 substantiated by the fact that SO₂ concentrations in the air coming from ocean side were
407 much lower than those coming from the continent (e.g., at BG_c site, average SO₂
408 concentration in the air mass from ocean and continent were 1.4 ppbv and 2.8 ppbv,
409 respectively) and supported by other studies at coastal site (*Yu et al., 2014*).

410 The CS values of NPF events are calculated as the mean CS value between 9:00 to
411 12:00 h (local time) of the day (Eq. 3). In general, CS in all NPF days were in the range
412 of $0.9\text{-}5.6 \times 10^{-2} \text{ s}^{-1}$ at urban sites, $0.3\text{-}8.6 \times 10^{-2} \text{ s}^{-1}$ at regional sites, $1.1\text{-}2.6 \times 10^{-2} \text{ s}^{-1}$ at
413 coastal/background sites and $0.9\text{-}1.1 \times 10^{-2} \text{ s}^{-1}$ during cruise measurement (see Table 3).
414 The upper limits of CS at urban and regional sites were far larger compared with those
415 at coastal/background sites and cruise measurement and at other sites in western
416 countries (Table 3), which further confirms the fact that NPF events can occur under
417 high aerosol loading in polluted areas in China (Wu *et al.*, 2007). On the other hand, the
418 lower limit of CS at different sites showed no obvious difference, indicating that there
419 are “clean case” NPF events even in these polluted urban areas (Wu *et al.*, 2007).

420 The GRs of newly formed particles (calculated from 15 nm to 30 nm) ranged from
421 4.2 to 18.1 nm h^{-1} at urban sites, 3.2 to 21 nm h^{-1} at regional sites, and 1.6 to 7.5 nm h^{-1}
422 ¹ at both coastal sites and cruise measurement (Table 3). The highest GR was found at
423 YF_r site (regional) with value of 21 nm h^{-1} . Average GRs at urban and regional sites
424 were about twice those at coastal sites and cruise measurement (Table 3), indicating
425 that the higher concentrations of gaseous precursors in the polluted areas not only favor
426 the formation of particles, but also accelerate the growth rate as long as the nucleation
427 particles are formed.

428 Both the CS and GR results in our study are comparable to other studies performed
429 in Beijing (Wu *et al.*, 2007), Back-garden (Yue *et al.*, 2013), and Xinken (Liu *et al.*,
430 2008), in China. CS values in our study are generally higher than those at European and
431 American sites and smaller than those at some sites in developing countries, such as
432 New Delhi (see Table 3). The GR values show no obvious differences between China
433 and other countries (both in developed and developing countries) at the same site types
434 (see Table 3).

435 **3.5 Evaluation of the contribution of NPF to potential CCN**

436 The basic idea to estimate the production of potential CCN from NPF events is
437 based on the assumption that particles larger than a certain diameter could be served as

438 CCN. As the newly formed particles consist mainly ammonium sulfate and secondary
439 organics (Yue *et al.*, 2010) and primary emission particles contain a lot of black carbon
440 and hydrophobic organics (Medalia and Rivin, 1982; Reid *et al.*, 2005), the κ value for
441 newly formed particles and primary emission particles may be of large difference. Some
442 previous studies in China have concluded that the average κ value of all ambient
443 particles is about 0.3 for many environments in China (Gunthe *et al.*, 2011; Yue *et al.*,
444 2010; Rose *et al.*, 2010), but few has provided the κ value of newly formed particles
445 in the atmosphere. In this study, the hygroscopicity parameter κ for the newly formed
446 particles is taken as 0.43 at about 100 nm based on the assumption of one third of
447 chemical components of these particles are organics and others were inorganics
448 (Gunthe *et al.*, 2011; Yue *et al.*, 2010). Therefore, the only task left is to achieve the
449 PND of newly formed particles.

450 In this study, mode fitting method is used to distinguish the newly formed particles
451 from others. Diurnal half-hourly average PND data are used for the log-normal fitting.
452 A total of three (or four) lognormal modes are achieved in the fitness exercise (see Eq.
453 1) on the PND data. These include up to two NPF modes (with initial diameter about
454 15-20 nm, which may grow up to 50 nm later), one Aitken mode (40-100 nm) as well
455 as one accumulation mode (100-500 nm). Figure 6 illustrates an example of the mode
456 fitting result at the site of KP_r, which is a typical regional site with high frequency of
457 NPF events. Half-hourly fitting results in the afternoon from 11:00-16:00 h at KP_r site
458 with two NPF modes and two pre-existing modes are shown in Figure 6. At the site of
459 KP_r, NPF events were observed to occur between mainly between 9:00 and 11:00 h
460 every day, resulting in a sharp and narrow nucleation mode peak at about 19 nm at 11:00
461 h (Figure 6). In the following five hours, the peak diameter of NPF mode gradually
462 grew from 19 to 50 nm, with the concentration of NPF mode decreasing from 7500 to
463 5000 cm⁻³ at the same time. Furthermore, when the peak diameters of these log-normal
464 distribution NPF modes reached 50 nm, there would be a large amount of particles with
465 diameter exceed 80 nm or even 100 nm. These particles were large enough to possibly
466 act as CCN under a certain S_c. The contribution of NPF to potential CCN production

467 can then be calculated by integrating the distribution of the NPF mode particle with
468 diameter larger than $D_{p,crit}$. As it is challenging to extract NPF mode when the NPF
469 peaks are submerged in the size distribution of ambient particles, in order to achieve
470 accurate fitness results, prominent NPF peak in the size distribution is required.
471 Therefore, our subsequent discussions are focused on the time period from 13:00 to
472 17:00 h in the afternoon, as the time is neither too early for the formation of new
473 particles, nor too late for primary emission to perform a dominate role in the ambient
474 PND.

475 The contributions of NPF and growth to potential CCN concentration in all
476 measurements are calculated through this approach. Results of this exercise are
477 illustrated in Table 4. Two values of super saturations are assumed here as 0.5% and
478 0.2%, with critical diameter of 50 nm and 91 nm for newly formed particles, and 60 nm
479 and 100 nm for other particles, respectively. Contributions of NPF to potential CCN
480 concentration varied greatly during different measurements, ranging from 0% to 66%
481 when S_c is 0.5, and 0% to 24% when S_c is 0.2 (Table 4). The highest values were found
482 in the summer at WX_u site. During summertime, the average contributions values at
483 urban and regional sites were 50% ($S_c = 0.5$) and 18% ($S_c = 0.2$), which were much
484 higher than those in other seasons. The strong oxidation condition in summer favors the
485 formation of new NPF as well as the growth of newly formed particles, accelerating the
486 newly formed particles to perform as CCN. On the contrary, the contribution is 0%
487 during two winter measurements, as no NPF events were observed during these two
488 measurements.

489 Weighted average contributions for different size types are roughly calculated.
490 Annual average contribution of NPF to CCN at urban, regional and coastal sites were
491 found to be 33%, 19%, 7% (at $S_c=0.5$), and 11%, 6%, 0% (at $S_c=0.2$), respectively. Good
492 correlation ($R^2=0.7$) between growth rate of NPF and contribution to CCN among all
493 sites was found, indicating that growth rates of NPF events are the decisive factor in
494 the conversion of newly formed particle to possible CCN (Yue *et al.*, 2011).

495 Although there were two NPF events during the cruise measurement, no

496 contribution to CCN concentration was found by any of these NPF events, because the
497 diameter of these secondary particles did not meet the critical diameter for CCN. *Zhang*
498 *et al.* (2012) demonstrated that NPF in marine environment is not likely to produce
499 particles of the size of CCN. Our study further confirms that the NPF events show little
500 impact on the concentration of CCN in the marine area near polluted continent. It may
501 need more than one day for the newly formed particles to perform as CCN.

502 In previous studies, people always use the CCN concentration enhancement factor
503 to describe the contribution of NPF events to corresponding CCN (*Yue et al., 2011*;
504 *Kuang et al., 2009*; *Lihavainen et al., 2003*). It is obtained by dividing the concentration
505 of CCN-sized particles after a NPF event by that prior to the event. The average CCN
506 enhancement factors after the NPF events at $S_c = 0.2$ ($D_{p,crit} = 100$ nm) were calculated
507 to be 1.5 at a remote site in Northern Finland (*Lihavainen et al., 2003*) and in the range
508 of 1.5-2.5 in Beijing (*Yue et al., 2011*). Similar conclusion was obtained in Botsalano,
509 but with great seasonal variation (*Laakso et al., 2013*). The factors in these studies are
510 higher than in our study because they only considered NPF days. The values would be
511 much lower and similar to our result if the enhancements were multiplied by the
512 frequencies of NPF events. Besides, the method used in these studies did not consider
513 the influence of primary emissions and change of boundary layer height on CCN
514 concentration (*Laakso et al., 2013*) and thus may overestimate the enhancements. In
515 our study, all the sites were away from main road and stationary sources, PNCs of
516 primary emission were not expected to change much during the focused time intervals.
517 Besides, the mode fit method has considered the non-NPF particles. Therefore, our
518 results are not influenced greatly by the primary emissions. However, the approach to
519 calculate the contribution of NPF to CCN also has some uncertainties and limitations.
520 First, we can only calculate the contribution to CCN production by the NPF event in
521 the same day. Some of the pre-existing particles before NPF events may also come from
522 the NPF in previous days, but these can only be recognized as pre-existing particles
523 rather than NPF particles through our approach. This is likely to result in
524 underestimation of the contribution. Second, even though our method has its advantage

525 on distinguish the nucleation particles from non-NPF particles, some non-NPF particles
526 may have a chance to be recognized as nucleation particle when we perform the
527 processing of diurnal average PNCs, which may lead to overestimation of results. Third,
528 as discussed above, the approach requires very clear NPF peaks in the size distributions
529 in order to achieve accurate fitness results. So the focusing time period is constrained
530 between 14:00 and 17:00 h, when the NPF mode is clear and evening rush hour has not
531 come. The contribution in the following hours or the following days cannot be precisely
532 calculated though this approach. As it is crucial to evaluate the contribution of NPF
533 events to CCN production in the following days, more studies on this field are needed
534 in the future. Nevertheless, based on field measurements, our work provides annual and
535 seasonal average contribution of NPF events to CCN production for the first time in
536 diversified Chinese atmosphere. The estimation of contribution of NPF events to
537 corresponding CCN might be particularly useful for the validation of global climate
538 models.

539 **4. Summary and conclusions**

540 This paper presents size-resolved measurements of submicron aerosol in the 15-
541 600 nm size range during the 15 individual field campaigns, taken between 2008 and
542 2011, at thirteen different sites in China. These sites include 5 urban sites, 4 regional
543 sites, 3 coastal/background sites and one ship cruise measurement, and are mainly
544 located within the three largest city clusters of China.

545 The particle number size distributions were fitted into three modes (nucleation,
546 Aitken, accumulation) at most of the sites. The median PNC at urban ($1.1\text{-}2.2 \times 10^4 \text{ cm}^{-3}$)
547 and regional sites ($0.8\text{-}1.5 \times 10^4 \text{ cm}^{-3}$) are two-times larger than those at coastal and
548 background ($0.4\text{-}0.6 \times 10^4 \text{ cm}^{-3}$) sites and cruise measurement ($0.5 \times 10^4 \text{ cm}^{-3}$).

549 Primary emission from road vehicles as well as regional biomass burning appears
550 to have a large contribution to the ambient PNCs. High emissions from road vehicles at
551 urban sites resulted in up to 10-times higher N_{25-100} than those of $N_{100-600}$. PNCs in both
552 size ranges were nearly identical at all other sites. Vehicular emissions at urban sites

553 and biomass burning emission at regional sites led to two concentration peaks in the
554 early morning and evening hours.

555 Regional secondary aerosol pollution is a main feature for the submicron aerosol
556 pollution in China. No obvious differences in the $N_{100-600}$ particles were observed
557 between urban and regional sites. Diurnal variations show a build-up of high
558 concentration accumulation belt at all the regional sites.

559 The occurrence frequencies of the NPF events in high aerosol-loading environment
560 of China were found to be higher than those in less aerosol-loading environments. High
561 gaseous precursors and strong oxidation at urban and regional sites not only favor the
562 formation of particles, but also accelerate the growth rate after the nucleation mode
563 particles are formed. The average GR of nucleation mode particles were $8.0-10.9 \text{ nm h}^{-1}$
564 1 at urban sites, $7.4-13.6 \text{ nm h}^{-1}$ at regional sites and $2.8-7.5 \text{ nm h}^{-1}$ at coastal sites and
565 cruise measurement. The NPF events in the less aerosol-loading environment were
566 found to be greatly influenced by pollutant transport.

567 Average contributions of NPF events to potential CCN are calculated in this study.
568 Contributions of NPF events to potential CCN at 0.2 super-saturation in the afternoon
569 of all measurement days were 11% and 6% at urban sites and regional sites, respectively.
570 On the other hand, NPF events at coastal sites and cruise measurement had little impact
571 on potential CCN.

572 Our study presents a unique dataset of aerosol size distributions and general
573 concepts of the features of submicron particle pollution along with the fundamental
574 drivers of particulate pollution in China. Besides, our estimation of contribution of NPF
575 events to corresponding CCN might be particularly useful for the validation of global
576 climate models.

577 **5. Acknowledgement**

578 This work was supported by the National Natural Science Foundation of China
579 (21025728 and 21190052), the National Basic Research Program of

580 China (2013CB228503) and the China Ministry of Environmental Protection's Special
581 Funds for Scientific Research on Public Welfare (201009002). Prashant Kumar, Jianfei
582 Peng and Min Hu thank the University of Surrey's International Relations Office for
583 the Santander Postgraduate Mobility Award that helped Jianfei Peng to visit University
584 of Surrey, UK, to develop this research article collaboratively.

585

586 **References**

- 587 Andreae, M. O.: The Aerosol Nucleation Puzzle, *Science*, 339, 911-912,
588 doi:10.1126/science.1233798, 2013.
- 589 Asmi, A., Wiedensohler, A., Laj, P., Fjaeraa, A. M., Sellegri, K., Birmili, W.,
590 Weingartner, E., Baltensperger, U., Zdimal, V., Zikova, N., Putaud, J. P., Marinoni,
591 A., Tunved, P., Hansson, H. C., Fiebig, M., Kivekäs, N., Lihavainen, H., Asmi, E.,
592 Ulevicius, V., Aalto, P. P., Swietlicki, E., Kristensson, A., Mihalopoulos, N.,
593 Kalivitis, N., Kalapov, I., Kiss, G., de Leeuw, G., Henzing, B., Harrison, R. M.,
594 Beddows, D., O'Dowd, C., Jennings, S. G., Flentje, H., Weinhold, K., Meinhardt, F.,
595 Ries, L., Kulmala, M.: Number size distributions and seasonality of submicron
596 particles in Europe 2008–2009, *Atmos. Chem. Phys.*, 11, 5505-5538,
597 doi:10.5194/acp-11-5505-2011, 2011a.
- 598 Asmi, E., Kivekas, N., Kerminen, V. M., Komppula, M., Hyvarinen, A. P., Hatakka, J.,
599 Viisanen, Y., and Lihavainen, H.: Secondary new particle formation in Northern
600 Finland Pallas site between the years 2000 and 2010, *Atmos. Chem. Phys.*, 11,
601 12959-12972, 2011b.
- 602 Bigi, A., and Ghermandi, G.: Particle Number Size Distribution and Weight
603 Concentration of Background Urban Aerosol in a Po Valley Site, *Water Air Soil*
604 *Poll.*, 220, 265-278, doi:10.1007/s11270-011-0752-6, 2011.
- 605 Borsos, T., Rimnacova, D., Zdimal, V., Smolik, J., Wagner, Z., Weidinger, T., Burkart,
606 J., Steiner, G., Reischl, G., Hitzemberger, R., Schwarz, J., and Salma, I.: Comparison
607 of particulate number concentrations in three Central European capital cities, *Sci.*
608 *Total Environ.*, 433, 418-426, 2012.
- 609 Boy, M., Kulmala, M., Ruuskanen, T. M., Pihlatie, M., Reissell, A., Aalto, P. P.,
610 Keronen, P., Dal Maso, M., Hellen, H., Hakola, H., Jansson, R., Hanke, M., and
611 Arnold, F.: Sulphuric acid closure and contribution to nucleation mode particle
612 growth. *Atmos. Chem. Phys.*, 5, 863-878, 2005.
- 613 Buseck, P. R., and Adachi, K.: Nanoparticles in the Atmosphere, *Elements*, 4, 389-394,
614 doi:10.2113/gselements.4.6.389, 2008.
- 615 Creamean, J. M., Ault, A. P., Ten Hoeve, J. E., Jacobson, M. Z., Roberts, G. C., and
616 Prather, K. A.: Measurements of Aerosol Chemistry during New Particle Formation
617 Events at a Remote Rural Mountain Site, *Environ. Sci. Technol.*, 45, 8208-8216,
618 2011.

619 Dal Maso, M., Kulmala, M., Riipinen, I., Wagner, R., Hussein, T., Aalto, P. P., and
620 Lehtinen, K. E. J.: Formation and growth of fresh atmospheric aerosols: eight years
621 of aerosol size distribution data from SMEAR II, Hyytiälä, Finland, *Boreal Environ.
622 Res.*, 10, 323-336, 2005.

623 Davidson, C. I., and Wu, Y. L.: Dry deposition of particles and vapors, in *Acid
624 Precipitation*, Vol. 3, S. E. Lindberg, A. L. Page, and S. A. Norton, eds., Springer-
625 Verlag, Berlin, pp. 103-209, 1990.

626 Du, J. F., Cheng, T. T., Zhang, M., Chen, J. M., He, Q. S., Wang, X. M., Zhang, R. J.,
627 Tao, J., Huang, G. H., Li, X., and Zha, S. P.: Aerosol Size Spectra and Particle
628 Formation Events at Urban Shanghai in Eastern China, *Aerosol Air Qual. Res.*,
629 12(6), 1362-1372, 2012.

630 Dunn, M. J., Jimenez, J. L., Baumgardner, D., Castro, T., McMurry, P. H., and Smith,
631 J. N.: Measurements of Mexico City nanoparticle size distributions: Observations
632 of new particle formation and growth, *Geophys. Res. Lett.*, 31, L10102,
633 doi:10.1029/2004GL019483, 2004.

634 Dusek, U., Frank, G. P., Hildebrandt, L., Curtius, J., Schneider, J., Walter, S., Chand,
635 D., Drewnick, F., Hings, S., Jung, D., Borrmann, S., and Andreae, M. O.: Size
636 Matters More Than Chemistry for Cloud-Nucleating Ability of Aerosol Particles,
637 *Science*, 312, 1375-1378, doi:10.1126/science.1125261, 2006.

638 Gao, J., Chai, F. H., Wang, T., and Wang, W. X.: Particle number size distribution and
639 new particle formation (NPF) in Lanzhou, Western China, *Particuology*, 9, 611-618,
640 2011.

641 Gong, Z. H., Lan, Z. J., Xue, L., Zeng, L. W., He, L. Y., and Huang, X. F.:
642 Characterization of submicron aerosols in the urban outflow of the central Pearl
643 River Delta region of China, *Frontiers of Environmental Science & Engineering*, 6,
644 725-733, 2012.

645 Gunthe, S. S., Rose, D., Su, H., Garland, R. M., Achtert, P., Nowak, A., Wiedensohler,
646 A., Kuwata, M., Takegawa, N., Kondo, Y., Hu, M., Shao, M., Zhu, T., Andreae, M.
647 O., and Pöschl, U.: Cloud condensation nuclei (CCN) from fresh and aged air
648 pollution in the megacity region of Beijing, *Atmos. Chem. Phys.*, 11, 11023-11039,
649 doi:10.5194/acp-11-11023-2011, 2011.

650 Guo, S., Hu, M., Wang, Z. B., Slanina, J., and Zhao, Y. L.: Size-resolved aerosol water-
651 soluble ionic compositions in the summer of Beijing: implication of regional
652 secondary formation, *Atmos. Chem. Phys.*, 10, 947-959, 2010.

653 Hamed, A., Joutsensaari, J., Mikkonen, S., Sogacheva, L., Dal Maso, M., Kulmala, M.,
654 Cavalli, F., Fuzzi, S., Facchini, M. C., Decesari, S., Mircea, M., Lehtinen, K. E. J.,
655 and Laaksonen, A.: Nucleation and growth of new particles in Po Valley, Italy,
656 *Atmos. Chem. Phys.*, 7, 355-376, 2007.

657 Harrison, R. M., Beddows, D. C. S., and Dall'Osto, M.: PMF Analysis of Wide-Range
658 Particle Size Spectra Collected on a Major Highway, *Environ. Sci. Technol.*, 45,
659 5522-5528 2011.

660 Heal, M. R., Kumar, P., and Harrison, R. M.: Particles, air quality, policy and health,
661 *Chem. Soc. Rev.*, 41, 6606-6630, 2012.

662 Herrmann, E., Ding, A. J., Kerminen, V. M., Petaja, T., Yang, X. Q., Sun, J. N., Qi, X.

663 M., Manninen, H., Hakala, J., Nieminen, T., Aalto, P. P., Kulmala, M., Fu, C. B.:
664 Aerosols and nucleation in eastern China: first insights from the new SORPES-NJU
665 station, *Atmos. Chem. Phys.*, 4, 2169-2183, 2014.

666 Hu, W. W., Hu, M., Yuan, B., Jimenez, J. L., Tang, Q., Peng, J. F., Hu, W., Shao, M.,
667 Wang, M., Zeng, L. M., Wu, Y. S., Gong, Z. H., Huang, X. F., and He, L. Y.: Insights
668 on organic aerosol aging and the influence of coal combustion at a regional receptor
669 site of central eastern China, *Atmos. Chem. Phys.*, 13, 10095-10112,
670 doi:10.5194/acp-13-10095-2013, 2013.

671 Huang, X. F., He, L. Y., Hu, M., Canagaratna, M. R., Kroll, J. H., Ng, N. L., Zhang, Y.
672 H., Lin, Y., Xue, L., Sun, T. L., Liu, X. G., Shao, M., Jayne, J. T., and Worsnop, D.
673 R.: Characterization of submicron aerosols at a rural site in Pearl River Delta of
674 China using an Aerodyne High-Resolution Aerosol Mass Spectrometer, *Atmos.*
675 *Chem. Phys.*, 11, 1865-1877, 2011.

676 Huang, X. F., He, L. Y., Xue, L., Sun, T. L., Zeng, L. W., Gong, Z. H., Hu, M., and
677 Zhu, T.: Highly time-resolved chemical characterization of atmospheric fine
678 particles during 2010 Shanghai World Expo, *Atmos. Chem. Phys.*, 12, 4897-4907,
679 2012.

680 Iida, K., Stolzenburg, M. R., McMurry, P. H., and Smith, J. N.: Estimating nanoparticle
681 growth rates from size-dependent charged fractions: Analysis of new particle
682 formation events in Mexico City, *J Geophys. Res.*, 113, D05207
683 doi: 10.1029/2007JD009260, 2008.

684 IPCC (Intergovernmental Panel on Climate Change): Climate Change 2007: The
685 Physical Science Basis. Contribution of Working Group I to the Fourth Assessment,
686 Report of the Intergovernmental Panel on Climate Change, Cambridge University
687 Press, Cambridge, United Kingdom, and New York, NY, USA..

688 Kerminen, V. M., Paramonov, M., Anttila, T., Riipinen, I., Fountoukis, C., Korhonen,
689 H., Asmi, E., Laakso, L., Lihavainen, H., Swietlicki, E., Svenningsson, B., Asmi,
690 A., Pandis, S. N., Kulmala, M., and Petaja, T.: Cloud condensation nuclei
691 production associated with atmospheric nucleation: a synthesis based on existing
692 literature and new results, *Atmos. Chem. Phys.*, 12, 12037-12059, 2012.

693 Kuang, C., McMurry, P. H., and McCormick, A. V.: Determination of cloud
694 condensation nuclei production from measured new particle formation events,
695 *Geophys. Res. Lett.*, 36, L09822, doi:10.1029/2009GL037584, 2009.

696 Kulmala, M., Dal Maso, M., Makela, J. M., Pirjola, L., Vakeva, M., Aalto, P.,
697 Miikkulainen, P., Hameri, K., O'Dowd, C. D.: On the formation, growth and
698 composition of nucleation mode particles. *Tellus B*, 53, 479-490, 2001.

699 Kulmala, M., Kontkanen, J., Junninen, H., Lehtipalo, K., Manninen, H. E., Nieminen,
700 T., Petaja, T., Sipila, M., Schobesberger, S., Rantala, P., Franchin, A., Jokinen, T.,
701 Jarvinen, E., Aijala, M., Kangasluoma, J., Hakala, J., Aalto, P. P., Paasonen, P.,
702 Mikkila, J., Vanhanen, J., Aalto, J., Hakola, H., Makkonen, U., Ruuskanen, T.,
703 Mauldin, R. L., Duplissy, J., Vehkamaki, H., Back, J., Kortelainen, A., Riipinen, I.,
704 Kurten, T., Johnston, M. V., Smith, J. N., Ehn, M., Mentel, T. F., Lehtinen, K. E. J.,
705 Laaksonen, A., Kerminen, V. M., Worsnop, D. R.: Direct observations of
706 atmospheric aerosol nucleation, *Science*, 339, 943-946,

707 doi:10.1126/science.1227385, 2013.

708 Kulmala, M., Petaja, T., Nieminen, T., Sipila, M., Manninen, H. E., Lehtipalo, K., Dal
709 Maso, M., Aalto, P. P., Junninen, H., Paasonen, P., Riipinen, I., Lehtinen, K. E. J.,
710 Laaksonen, A., Kerminen, V. M.: Measurement of the nucleation of atmospheric
711 aerosol particles, *Nature Protoc.*, 7,1651-1667, 2012.

712 Kumar, P., Morawska, L., Birmili, W., Paasonen, P., Hu, M., Kulmala, M., Harrison, R.
713 M., Norford, L., and Britter, R.: Ultrafine particles in cities, *Environ. Int.*, 66, 1-10,
714 2014.

715 Kumar, P., Morawska, L., and Harrison, R. M.: Nanoparticles in European cities and
716 associated health impacts. In *Urban Air Quality in Europe: The Handbook of
717 Environmental Chemistry* (Editor Viana, M.). Springer Berlin Heidelberg, Volume
718 26, pp. 339-365, http://dx.doi.org/10.1007/698_2012_161, 2013a.

719 Kumar, P., Pirjola, L., Ketzler, M., and Harrison, R. M.: Nanoparticle emissions from 11
720 non-vehicle exhaust sources - A review, *Atmos. Environ.*, 67, 252-277, 2013b.

721 Kumar, P., Robins, A., Vardoulakis, S., and Britter, R.: A review of the characteristics
722 of nanoparticles in the urban atmosphere and the prospects for developing
723 regulatory controls, *Atmos. Environ.*, 44, 5035-5052, 2010.

724 Kumar, P., Gurjar, B.R., Nagpure, A., and Harrison, R. H.: Preliminary estimates of
725 particle number emissions from road vehicles in megacity Delhi and associated
726 health impacts. *Environ. Sci. Technol.*, 45, 5514-5521, 2011.

727 Laakso, L., Merikanto, J., Vakkari, V., Laakso, H., Kulmala, M., Molefe, M., Kgabi, N.,
728 Mabaso, D., Carslaw, K. S., Spracklen, D. V., Lee, L. A., Reddington, C. L., and
729 Kerminen, V. M.: Boundary layer nucleation as a source of new CCN in savannah
730 environment, *Atmos. Chem. Phys.*, 13, 1957-1972, doi:10.5194/acp-13-1957-2013,
731 2013.

732 Li, J., Zhuang, G. S., Huang, K., Lin, Y. F., Xu, C., and Yu, S. L.: Characteristics and
733 sources of air-borne particulate in Urumqi, China, the upstream area of Asia dust,
734 *Atmos. Environ.*, 42, 776-787, 2008.

735 Lihavainen, H., Kerminen, V. M., Komppula, M., Hatakka, J., Aaltonen, V., Kulmala,
736 M., and Viisanen, Y.: Production of "potential" cloud condensation nuclei associated
737 with atmospheric new-particle formation in northern Finland, *J Geophys. Res.*, 108,
738 4782, doi:10.1029/2003jd003887, 2003.

739 Lin, M., Holloway, T., Oki, T., Streets, D. G., and Richter, A.: Multi-scale model
740 analysis of boundary layer ozone over East Asia, *Atmos. Chem. Phys.*, 9, 3277-
741 3301, 2009.

742 Lin, P., Hu, M., Wu, Z., Niu, Y., and Zhu, T.: Marine aerosol size distributions in the
743 springtime over China adjacent seas, *Atmos. Environ.*, 41, 6784-6796, 2007.

744 Liu, S., Hu, M., Wu, Z. J., Wehner, B., Wiedensohler, A., and Cheng, Y. F.: Aerosol
745 number size distribution and new particle formation at a rural/coastal site in Pearl
746 River Delta (PRD) of China, *Atmos. Environ.*, 42, 6275-6283, 2008.

747 Medalia, A. I., and Rivin, D.: Particulate carbon and other components of soot and
748 carbon-black, *Carbon*, 20, 481-492, doi:10.1016/0008-6223(82)90084-7, 1982.

749 Merikanto, J., Spracklen, D. V., Mann, G. W., Pickering, S. J., and Carslaw, K. S.:
750 Impact of nucleation on global CCN, *Atmos. Chem. Phys.*, 9, 8601-8616, 2009.

751 Moffet, R. C., and Prather, K. A.: In-situ measurements of the mixing state and optical
752 properties of soot with implications for radiative forcing estimates, *P Natl. Acad.*
753 *Sci. USA*, 106, 11872-11877, 2009.

754 Monkkonen, P., Koponen, I. K., Lehtinen, K. E. J., Hameri, K., Uma, R., and Kulmala,
755 M.: Measurements in a highly polluted Asian mega city: observations of aerosol
756 number size distribution, modal parameters and nucleation events, *Atmos. Chem.*
757 *Phys.*, 5, 57-66, 2005.

758 Nel, A., Xia, T., Madler, L., and Li, N.: Toxic potential of materials at the nanolevel,
759 *Science*, 311, 622-627, 2006.

760 Petters, M. D., and Kreidenweis, S. M.: A single parameter representation of
761 hygroscopic growth and cloud condensation nucleus activity, *Atmos. Chem. Phys.*,
762 7, 1961-1971, 2007.

763 Reid, J. S., Koppmann, R., Eck, T. F., and Eleuterio, D. P.: A review of biomass burning
764 emissions part II: intensive physical properties of biomass burning particles, *Atmos.*
765 *Chem. Phys.*, 5, 799-825, 2005.

766 Salma, I., Borsos, T., Weidinger, T., Aalto, P., Hussein, T., Dal Maso, M., and Kulmala,
767 M.: Production, growth and properties of ultrafine atmospheric aerosol particles in
768 an urban environment, *Atmos. Chem. Phys.*, 13, 1339-1353, 2011.

769 See, S. W., Balasubramanian, R., and Wang, W.: A study of the physical, chemical, and
770 optical properties of ambient aerosol particles in Southeast Asia during hazy and
771 nonhazy days, *J Geophys. Res.*, 111, D10S08, doi:10.1029/2005jd006180, 2006.

772 Seinfeld, J. H., and Pandis, S. N.: *Atmos. Chem. Phys.*. From air pollution to climate
773 change, John Wiley & Sons New York, 429-443, 1998.

774 Shen, X. J., Sun, J. Y., Zhang, Y. M., Wehner, B., Nowak, A., Tuch, T., Zhang, X. C.,
775 Wang, T. T., Zhou, H. G., Zhang, X. L., Dong, F., Birmili, W., and Wiedensohler,
776 A.: First long-term study of particle number size distributions and new particle
777 formation events of regional aerosol in the North China Plain, *Atmos. Chem. Phys.*,
778 11, 1565-1580, doi:10.5194/acp-11-1565-2011, 2011.

779 Reid, J. S., Eck, T. F., Christopher, S. A., Koppmann, R., Dubovik, O., Eleuterio, D. P.,
780 Holben, B. N., Reid, E. A., and Zhang, J.: A review of biomass burning emissions
781 part III: intensive optical properties of biomass burning particles, *Atmos. Chem.*
782 *Phys.*, 5, 827-849, 2005.

783 Rose, D., Nowak, A., Achtert, P., Wiedensohler, A., Hu, M., Shao, M., Zhang, Y.,
784 Andreae, M. O., and Poschl, U.: Cloud condensation nuclei in polluted air and
785 biomass burning smoke near the mega-city Guangzhou, China - Part 1: Size-
786 resolved measurements and implications for the modeling of aerosol particle
787 hygroscopicity and CCN activity, *Atmos. Chem. Phys.*, 10, 3365-3383, 2010.

788 Wang, Z. B., Hu, M., Sun, J. Y., Wu, Z. J., Yue, D. L., Shen, X. J., Zhang, Y. M., Pei,
789 X. Y., Cheng, Y. F., and Wiedensohler, A.: Characteristics of regional new particle
790 formation in urban and regional background environments in the North China Plain,
791 *Atmos. Chem. Phys.*, 13, 12495-12506, 10.5194/acp-13-12495-2013, 2013a.

792 Wang, Z. B., Hu, M., Wu, Z. J., and Yue, D. L.: Research on the Formation Mechanisms
793 of New Particles in the Atmosphere, *Acta Chim. Sinica*, 71, 519-527,
794 10.6023/a12121062, 2013b.

795 Wang, Z. B., Hu, M., Yue, D. L., He, L. Y., Huang, X. F., Yang, Q., Zheng, J., Zhang,
796 R. Y., and Zhang, Y. H.: New particle formation in the presence of a strong biomass
797 burning episode at a downwind rural site in PRD, China, *Tellus B*, 65, 19965,
798 <http://dx.doi.org/10.3402/tellusb.v65i0.19965>, 2013c.

799 Wehner, B., and Wiedensohler, A.: Long term measurements of submicrometer urban
800 aerosols: statistical analysis for correlations with meteorological conditions and
801 trace gases, *Atmos. Chem. Phys.*, 3, 867-879, 2003.

802 Wehner, B., Wiedensohler, A., Tuch, T. M., Wu, Z. J., Hu, M., Slanina, J., and Kiang,
803 C. S.: Variability of the aerosol number size distribution in Beijing, China: New
804 particle formation, dust storms, and high continental background, *Geophys. Res.
805 Lett.*, 31, L22108, DOI: 10.1029/2004GL021596, 2004.

806 WHO: Review 5 of evidence on health aspects of air pollution – REVIHAAP. World
807 Health Organisation, Regional Office for Europe, available at:
808 http://www.euro.who.int/__data/assets/pdf_file/0020/182432/e96762-final.pdf
809 (last access: 5 June 2014), 2013.

810 Wiedensohler, A., Cheng, Y. F., Nowak, A., Wehner, B., Achtert, P., Berghof, M.,
811 Birmili, W., Wu, Z. J., Hu, M., Zhu, T., Takegawa, N., Kita, K., Kondo, Y., Lou, S.
812 R., Hofzumahaus, A., Holland, F., Wahner, A., Gunthe, S. S., Rose, D., Su, H., and
813 Poschl, U.: Rapid aerosol particle growth and increase of cloud condensation
814 nucleus activity by secondary aerosol formation and condensation: A case study for
815 regional air pollution in northeastern China, *J Geophys. Res.*, 114, D00G08,
816 DOI: 10.1029/2008JD010884, 2009.

817 Willeke, K. and Baron, P. A.: *Aerosol Measurement Principles, Techniques, and
818 Applications*, Van Nostrand Reinhold, Hoboken, NJ, 1993.

819 Wu, Z.J., Hu, M., Lin, P., Liu, S., Wehner, B., and Wiedensohler, A.: Particle number
820 size distribution in the urban atmosphere of Beijing, China, *Atmos. Environ.*, 42,
821 7967-7980, 2008.

822 Wu, Z. J., Hu, M., Liu, S., Wehner, B., Bauer, S., Ssling, A. M., Wiedensohler, A.,
823 Petaja, T., Dal Maso, M., and Kulmala, M.: New particle formation in Beijing,
824 China: Statistical analysis of a 1-year data set, *J Geophys. Res.*, 112, D09209,
825 DOI: 10.1029/2006JD007406, 2007.

826 Xu, P., Chen, Y. F., and Ye, X. J.: Haze, air pollution, and health in China, *Lancet*, 382,
827 2067-2067, 2013.

828 Yli-Juuti, T., Riipinen, I., Aalto, P. P., Nieminen, T., Maenhaut, W., Janssens, I. A.,
829 Claeys, M., Salma, I., Ocskay, R., Hoffer, A., Imre, K., and Kulmala, M.:
830 Characteristics of new particle formation events and cluster ions at K-puszta,
831 Hungary, *Boreal Environ. Res.*, 14, 683-698, 2009.

832 Yu, F., Luo, G., Liu, X., Easter, R. C., Ma, X., and Ghan, S. J.: Indirect radiative forcing
833 by ion-mediated nucleation of aerosol, *Atmos. Chem. Phys.*, 12, 11451-11463, 2012.

834 Yu, H., Hallar, A.G., You, Y., Sedlacek, A., Springston, S., Kanawade, V.P., Lee, Y.N.,
835 Wang, J., Kuang, C.G., McGraw, R.L., McCubbin, I., Mikkila, J., Lee, S.H.: Sub-
836 3nm particles observed at the coastal and continental sites in the United States, *J
837 Geophys. Res.*, 119, 860-879, 2014.

838 Yue, D. L., Hu, M., Wang, Z. B., Wen, M. T., Guo, S., Zhong, L. J., Wiedensohler, A.,

839 and Zhang, Y. H.: Comparison of particle number size distributions and new particle
840 formation between the urban and rural sites in the PRD region, China, *Atmos.*
841 *Environ.*, 76, 181-188, 2013.

842 Yue, D. L., Hu, M., Zhang, R. Y., Wu, Z. J., Su, H., Wang, Z. B., Peng, J. F., He, L. Y.,
843 Huang, X. F., Gong, Y. G., and Wiedensohler, A.: Potential contribution of new
844 particle formation to cloud condensation nuclei in Beijing, *Atmos. Environ.*, 45,
845 6070-6077, 2011.

846 Yue, D. L., Hu, M., Zhang, R. Y., Wang, Z. B., Zheng, J., Wu, Z. J., Wiedensohler, A.,
847 He, L. Y., Huang, X. F., and Zhu, T.: The roles of sulfuric acid in new particle
848 formation and growth in the mega-city of Beijing, *Atmos. Chem. Phys.*, 10, 4953-
849 4960, 2010.

850 Zhang, R. Y.: Getting to the Critical Nucleus of Aerosol Formation, *Science*, 328, 1366-
851 1367, 2010.

852 Zhang, R. Y., Khalizov, A., Wang, L., Hu, M., and Xu, W.: Nucleation and Growth of
853 Nanoparticles in the Atmosphere, *Chem. Rev.*, 112, 1957-2011, 2012.

854 Zhang, Y. H., Hu, M., Zhong, L. J., Wiedensohler, A., Liu, S. C., Andreae, M. O., Wang,
855 W., and Fan, S. J.: Regional Integrated Experiments on Air Quality over Pearl River
856 Delta 2004 (PRIDE-PRD2004): Overview, *Atmos. Environ.*, 42, 6157-6173, 2008.

857 **Table 1.** Summary of information providing description of sampling periods at each
858 measurement site. Please note that the words in parenthesis against each site represent
859 a short name of each site, and subscripts u, r, c and s indicate urban, regional, coastal
860 /background and cruise site types, respectively.

Type	Sites	Coordinates	Sampling period	Valid data
Urban	Guangzhou (GZ _u)	23.13° N, 113.26° E	Nov.12-29, 2010	4766
	Shanghai (SH _u)	31.23° N, 21.53° E	Apr.15-Jun.22, 2010	18658
	Urumchi (UC _u)	87.58° N, 43.83° E	May 16-Jun.2, 2008	4835
	Wuxi (WX _u)	31.56° N, 120.29° E	Jul.21-Aug.7, 2010 Jan.1-Jan.14, 2011	4769 4926
	Jinhua (JH _u)	29.1 °N, 119.69 °E	Oct.29-Nov.28, 2011	7776
Regional	Heshan (HS _r)	22.71 °N, 112.93 °E	Nov.12-29, 2010	4921
	Kaiping (KP _r)	22.33 °N, 112.54 °E	Oct.18-Nov.17, 2008	8465
	Jiaxing (JX _r)	30.8 °N, 120.8 °E	Jun.28-Jul.15, 2010 Dec.5-22, 2010	4564 4030
	Yufa (YF _r)	39.51 °N, 116.3 °E	Oct.5-31, 2007	5182
Coastal/ Background	Baguang (BG _c)	22.65 °N, 114.54 °E	Oct.25-Dec.3, 2009	5895
	Wenling (WL _c)	28.40 °N, 121.61 °E	Oct.30-Nov.28, 2011	7064
	Changdao (CD _c)	37.99 °N, 120.70 °E	Mar.19-Apr.24, 2011	10338
Cruise	East China sea (ES _s)	-	Mar.18-Apr.8, 2011	5015

861

862 **Table 2.** Particle diameter, percentile of total PNCs and modal fit parameters for median size distributions at each site. σ is the geometric standard
863 deviation of the mode, N_m is the mode number concentration, $D_{p,m}$ is the geometric mean diameter of the fitted log-normal mode.

Type	Sites	Peak diameter (nm)	Number Concentration (cm ⁻³)						Fitted mode 1			Fitted mode 2			Fitted mode 3		
			Average	5%	16%	50%	84%	95%	$D_{p,m}$ (nm)	N_m (cm ⁻³)	σ	$D_{p,m}$ (nm)	N_m (cm ⁻³)	σ	$D_{p,m}$ (nm)	N_m (cm ⁻³)	σ
Urban	GZ _u	85	13716	5222	6939	11563	20192	29838	166	3078	1.60	65	5404	1.72	17	5621	1.82
	SH _u	40	12931	4195	5903	10560	19746	28986	218	917	1.49	71	5863	1.7	25	4449	1.55
	UR _u	24	28421	6663	10977	22415	45214	70341	146	555	1.89	59	7122	1.83	24	18910	1.73
	WX _{u_win}	52	19465	5818	8556	16046	29533	47583	142	4972	1.60	63	9878	1.67	29	1250	1.33
	WX _{u_sum}	73	17396	7710	10572	16051	23794	31408	154	2092	1.61	61	7844	1.6	23	7473	1.59
	JH _u	115	14331	5029	6848	12809	21328	29956	329	206	1.23	116	10753	1.71	36	1892	1.52
Regional	HS _r	72	16076	7548	9635	15084	22230	27898	134	5784	1.61	59	9252	1.63	-	-	-
	KP _r	93	11170	2587	4177	7900	16520	32707	327	311	1.40	95	6883	1.81	17	1280	1.76
	JX _{r_sum}	68	16593	5320	7799	13033	23059	40126	197	1482	1.56	84	5560	1.56	25	7690	1.86
	JX _{r_win}	87	13610	3588	5700	11737	20917	30128	138	4946	1.59	74	2460	1.38	38	4451	1.6
	YF _r	123	10195	2259	4033	8761	15610	23455	150	5715	1.83	66	1831	1.58	26	1436	1.56
Coastal/ background	BG _c	90	7163	1885	3233	5874	10401	16519	211	1124	1.50	83	3798	1.66	35	924	1.37
	WL _c	73	5661	992	1659	3941	10207	16108	192	1413	1.63	68	2275	1.63	31	270	1.37
	CD _c	70	6629	1610	2594	5743	10451	14902	148	2247	1.67	57	3479	1.71	-	-	-
Cruise	ES _s	88	5571	1450	2259	4618	8391	17276	132	2123	1.55	59	2484	1.62	-	-	-

864

Table 3. Summary of parameters of NPF events at different sites.

Site	Type	Country	Season	CS($\times 10^{-2} \text{ s}^{-1}$)*	GR (nm h ⁻¹)*	Source
WX_u	Urban	China	Summer	1.7 (0.9-2.8)	10.4 (6.2-13.3)	This study
			Winter	None	None	This study
SH_u	Urban	China	Summer	2.0 (1.0-3.3)	8.0 (4.2-12)	This study
GZ_u	Urban	China	Autumn	3.9 (2.6-5.6)	10.9 (7.3-18.1)	This study
JH_u	Urban	China	Autumn	None	None	This study
UR_u	Urban	China	Spring	1.6 (1.0-2.6)	-	This study
Beijing	Urban	China	Whole year	0.6-6.1	0.1-11.2	(Wu <i>et al.</i> , 2007)
Lanzhou	Suburban	China	Summer	1.6 (0.9-2.4)	4.4 (1.4-17.0)	(Gao <i>et al.</i> , 2011)
Mexico City	urban	Mexico	Spring	-	0.5-9	(Dunn <i>et al.</i> , 2004)
Tecamac	Suburban	Mexico	Spring	-	15-40	(Iida <i>et al.</i> , 2008)
New Delhi	Urban	India	Autumn	5-7	15.0 (11.6-18.1)	(Monkkonen <i>et al.</i> , 2005)
Budapest	Urban	Hungary	Whole year	1.2	7.2 (2.0-13.3)	(Salma <i>et al.</i> , 2011)
Po Valley	Urban	Italy	Whole year	1.0 (0.4-1.8)	6.8 (4.2-8.0)	(Hamed <i>et al.</i> , 2007)
JX_r	Regional	China	Summer	2.2 (1.1-4.1)	13.6 (7.9-19.6)	This study
			Winter	None	None	This study
YF_r	Regional	China	Summer	2.7 (0.5-5.3)	12.3 (8.6-21)	This study
HS_r	Regional	China	Autumn	None	None	This study
KP_r	Regional	China	Autumn	2.5 (0.3-8.6)	7.4 (3.2-13.5)	This study
Back-garden	Regional	China	Summer	2.6 (2.3-3.3)	12.1 (4.0-22.7)	(Yue <i>et al.</i> , 2013)
Xinken	Regional	China	Autumn	-	8.3 (2.2-19.8)	(Liu <i>et al.</i> , 2008)
K-puszta	rural	Hungary	Summer	0.5 (0.06-1.4)	6.1 (2.2-14.4)	(Yli-Juuti <i>et al.</i> , 2009)
WL_c	Coastal	China	Autumn	2.6	7.5	This study
BG_c	Coastal	China	Autumn	1.4 (1.0-1.8)	4.5 (3.2-7.5)	This study
CD_c	Coastal	China	Spring	2.0 (1.9-2.1)	5.7 (4.5-6.8)	This study

ES_s	Marine	China	Spring	0.9 (0.8-1.1)	2.8 (1.6-3.9)	This study
Shangdianzi	Background	China	Whole year	2	4.3 (0.3-14.5)	(<i>Shen et al.</i> , 2011)
Yellow Sea	Marine	China	Spring	-	3.4	(<i>Lin et al.</i> , 2007)
Foresthill	Remote	American	Winter	-	2-8	(<i>Creamean et al.</i> , 2011)
Hyytiala	Forest	Finland	Whole year	0.2 (0.04-0.8)	3.0 (0.2-12)	(<i>Dal Maso et al.</i> , 2005)

866 * The values outside the bracket represent the average CS or GR; the values inside the bracket
867 represent the maximum and minimum CS or GR observed at each site; “none” means that there is
868 no NPF events found in the whole measurement; “-“ means that the GR value cannot be calculated
869 (only for the site of UR_u), or there is no such information in the reference paper.

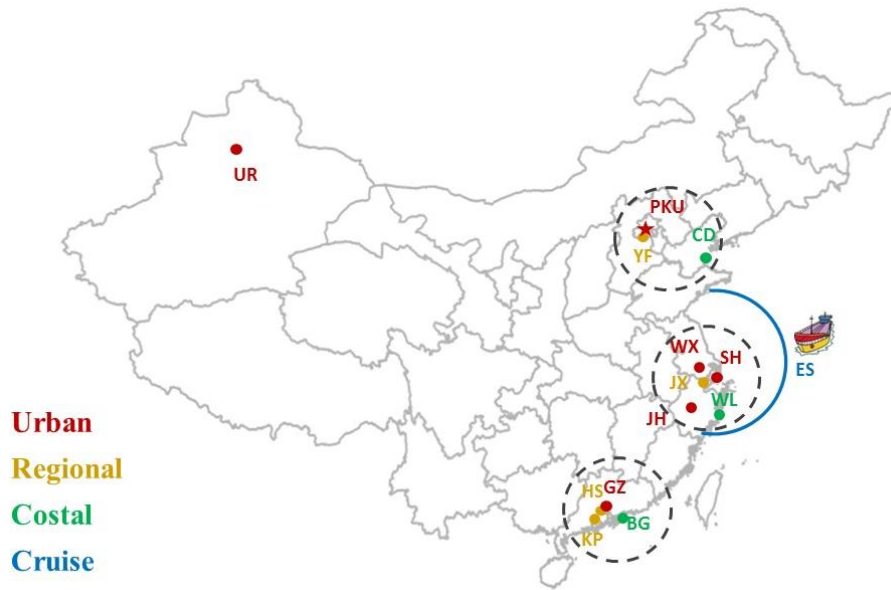
870 **Table 4.** Summary of contribution of NPF events to potential CCN during the time
 871 between 14:00 to 17:00 in all measurements.

	Spring		Summer		Autumn		Winter	
	S _c =0.5	S _c =0.2	S _c =0.5	S _c =0.2	S _c =0.5	S _c =0.2	S _c =0.5	S _c =0.2
Urban	33%	6%	66%	26%	31%	9%	0%	0%
Regional	-	-	57%	23%	30%	6%	0%	0%
Coastal	10%	<1%		-	8%	<1%	-	-
Cruise	<1%	<1%	-	-	-	-	-	-

872 “-” represents that there is no measurement at that type of sites in the certain season; “0%” represent
 873 that there is no NPF event found in the measurement; “<1%” represent that there are NPF events
 874 found in the measurement, but the relative contributions of these NPF events to the total CCN
 875 concentration are smaller than 1%.

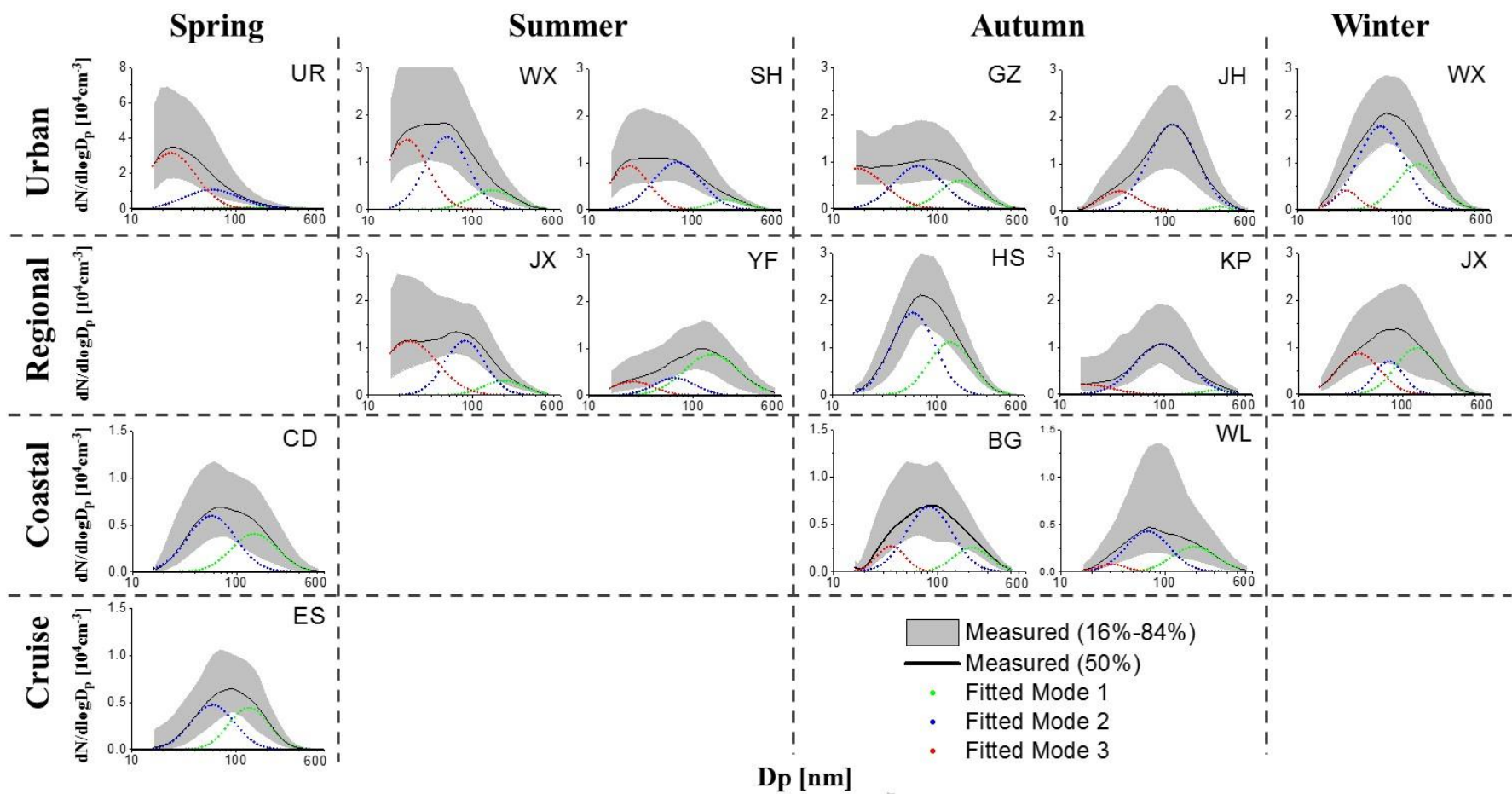
876

877



878

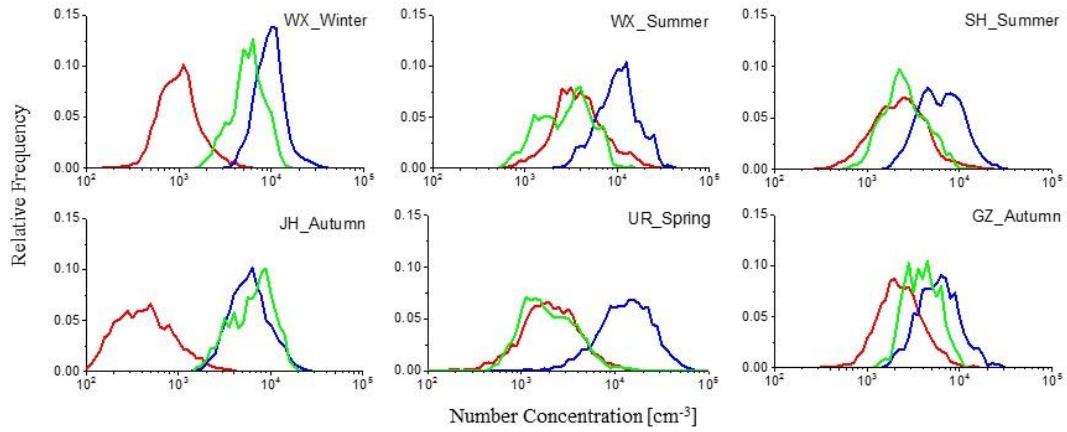
879 **Figure 1.** The location of all the thirteen measurement sites. Red, yellow, green and
 880 blue color dots represent the site type (urban, regional, coastal and cruise. Black circles
 881 show the three largest urban areas in China.



882

883 **Figure 2.** Median distribution (solid black line), 16th and 84th percentile distribution (shaded areas) and fitted mode (green, blue and red scatter

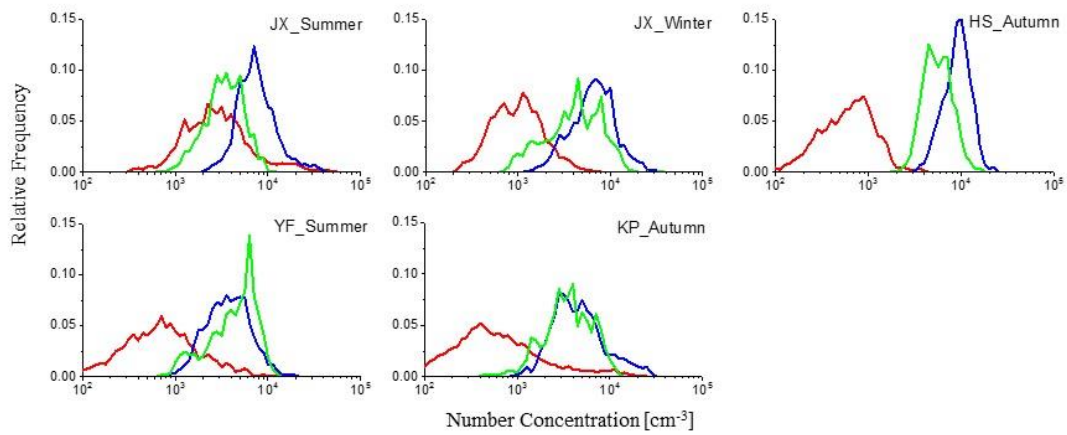
884 dots) at all the measurement sites.



885

886

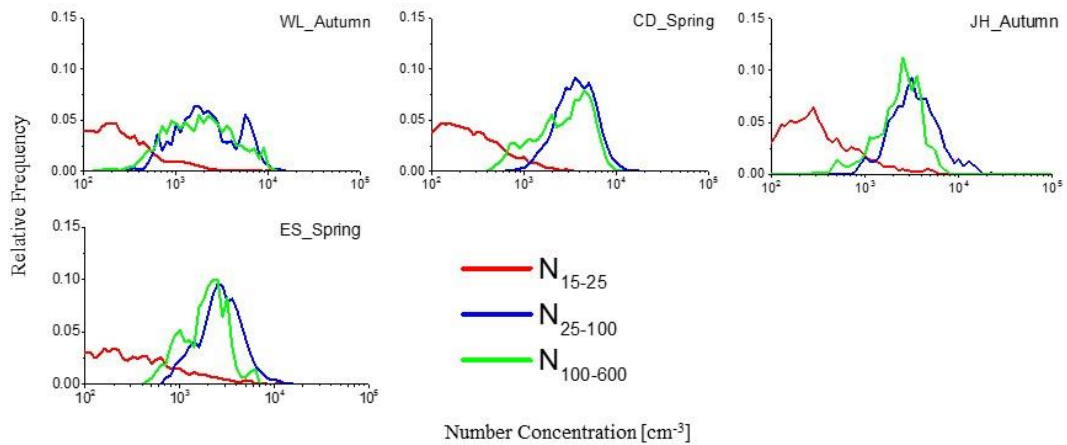
(a)



887

888

(b)



889

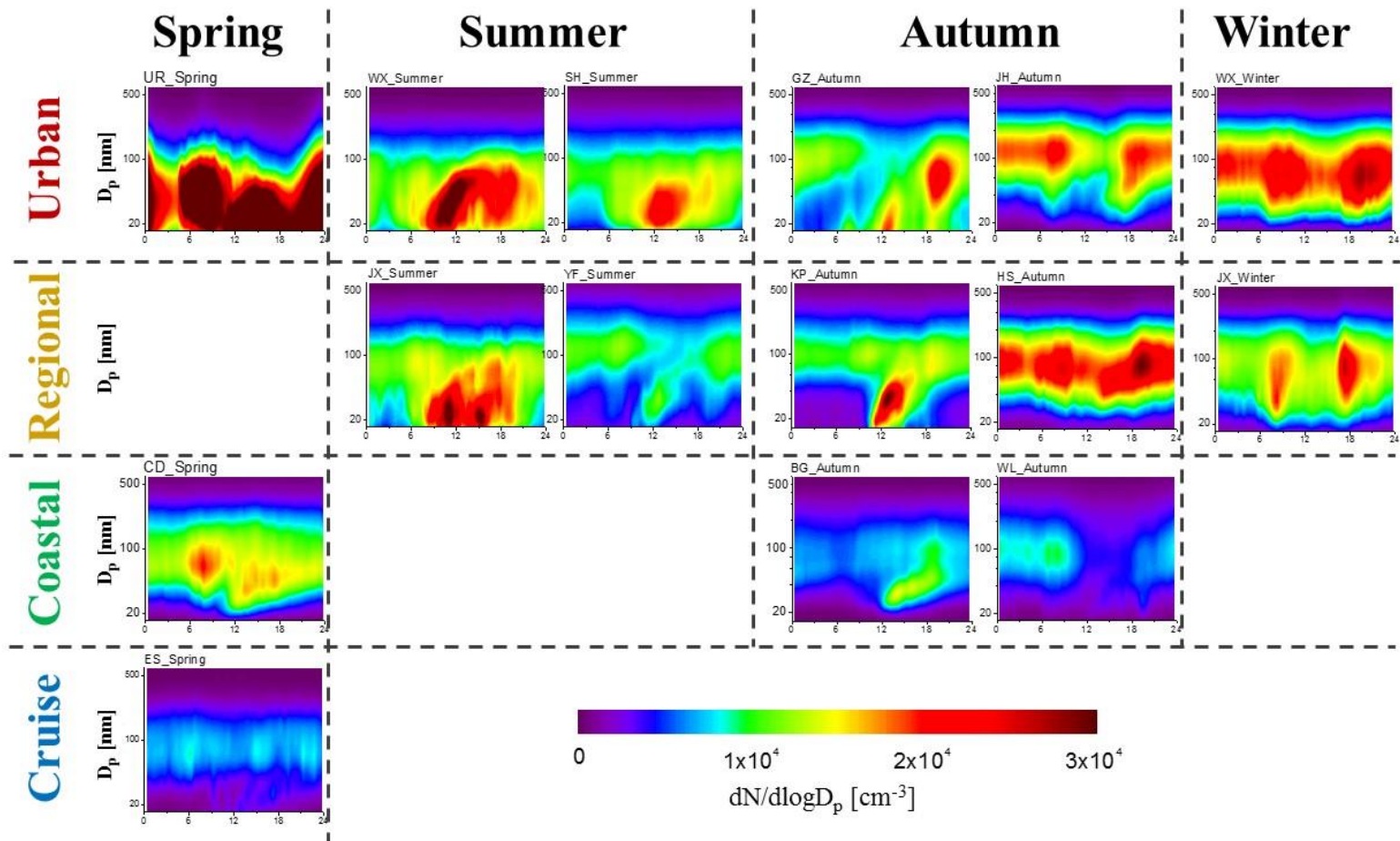
890

(c)

891 **Figure 3.** Distribution of PNC in different size ranges at (a) urban sites, (b) regional

892 sites, (c) coastal sites and ship measurement. The red, blue and green line represents the

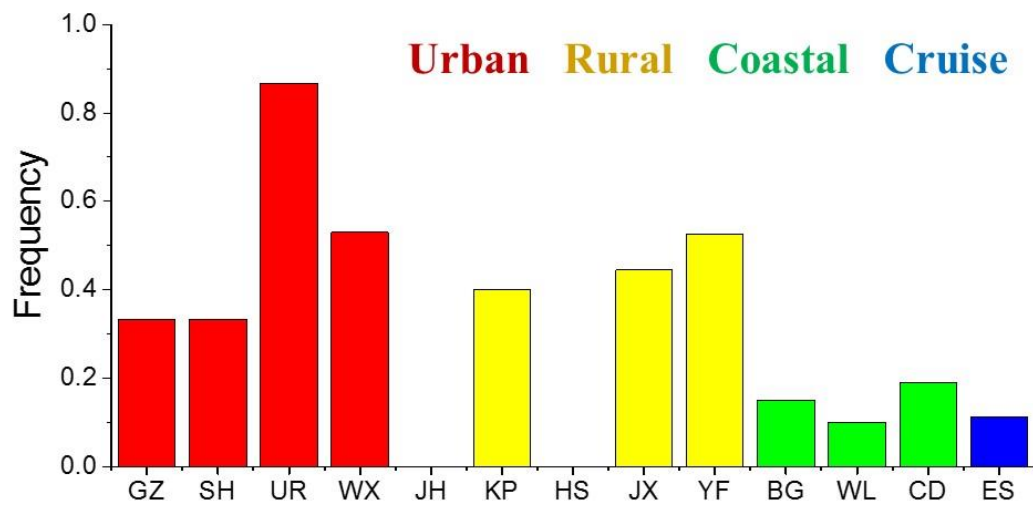
893 distribution of N_{15-25} , N_{25-100} and $N_{100-600}$, respectively.



894

895 **Figure 4.** Diurnal variation of PNDs during measurements at different types of sites during different seasons. The color represents $dN/d\log D_p$

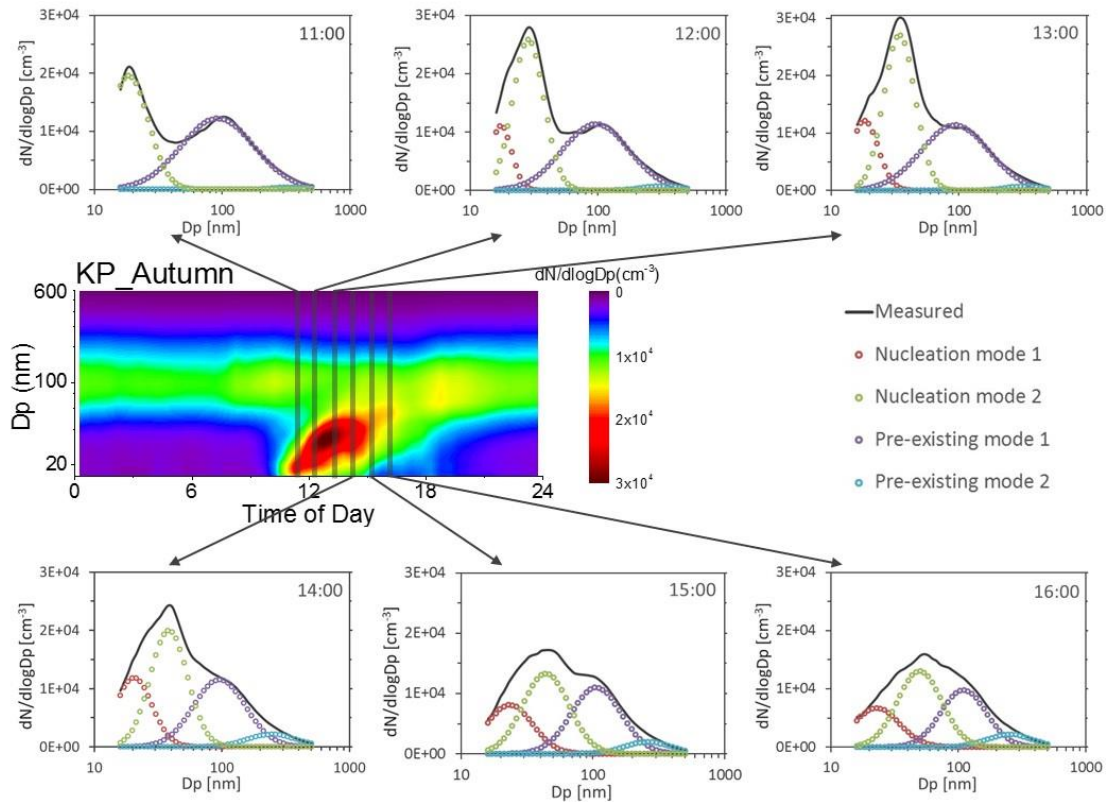
896 (cm^{-3}). All diurnal variation figures use the same axis and color bar.



897

898 **Figure 5.** Frequencies of NPF events at different sites. The color of red, yellow, green and blue
 899 represent the site type of urban, rural, coastal and cruise, respectively.

900



901

902 **Figure 6.** Lognormal fitting result of diurnal average PND at KP_r site. The six line and
 903 symbol pictures show the mode fit results for the diurnal variation from 11:00 to 16:00
 904 at KP_r site. Totally two nucleation modes and two pre-existing modes are found by
 905 mode fitting.